

## FARA

### A Fast Artifact Recovery Algorithm with Optimum Stimulation Waveform for Single-Cell Resolution Massively Parallel Neural Interfaces

Brash, Rohan ; Serdijn, Wouter; Muratore, Dante G.

#### DOI

[10.1109/ISCAS48785.2022.9937814](https://doi.org/10.1109/ISCAS48785.2022.9937814)

#### Publication date

2022

#### Document Version

Final published version

#### Published in

Proceedings of the 2022 IEEE International Symposium on Circuits and Systems (ISCAS)

#### Citation (APA)

Brash, R., Serdijn, W., & Muratore, D. G. (2022). FARA: A Fast Artifact Recovery Algorithm with Optimum Stimulation Waveform for Single-Cell Resolution Massively Parallel Neural Interfaces. In *Proceedings of the 2022 IEEE International Symposium on Circuits and Systems (ISCAS)* (pp. 190-194). (Proceedings - IEEE International Symposium on Circuits and Systems; Vol. 2022-May). IEEE.  
<https://doi.org/10.1109/ISCAS48785.2022.9937814>

#### Important note

To cite this publication, please use the final published version (if applicable).  
Please check the document version above.

#### Copyright

Other than for strictly personal use, it is not permitted to download, forward or distribute the text or part of it, without the consent of the author(s) and/or copyright holder(s), unless the work is under an open content license such as Creative Commons.

#### Takedown policy

Please contact us and provide details if you believe this document breaches copyrights.  
We will remove access to the work immediately and investigate your claim.

***Green Open Access added to TU Delft Institutional Repository***

***'You share, we take care!' - Taverne project***

**<https://www.openaccess.nl/en/you-share-we-take-care>**

Otherwise as indicated in the copyright section: the publisher is the copyright holder of this work and the author uses the Dutch legislation to make this work public.

# FARA: A Fast Artifact Recovery Algorithm with Optimum Stimulation Waveform for Single-Cell Resolution Massively Parallel Neural Interfaces

Rohan Brash, Wouter Serdijn, Dante G. Muratore

Department of Microelectronics, Delft University of Technology, The Netherlands

**Abstract**—This paper introduces a fast artifact recovery algorithm (FARA) that uses electrochemical impedance spectroscopy to model the electrode-tissue interface and design an optimum stimulation waveform to minimize the residual artifact duration in single-cell resolution neural interfaces. Results in saline solution with a custom PCB and a 30  $\mu\text{m}$  diameter microelectrode array show a worst case artifact recovery time of 160  $\mu\text{s}$  when measured from the end of the working phase (anodic 500 nA, 250  $\mu\text{s}$ ). On average, the proposed algorithm provides an 81% improvement over a triphasic charge-balanced stimulation waveform.

## I. INTRODUCTION

Future neural interfaces will be able to modulate the nervous system at single-cell resolution over a large population of cells to provide better clinical and scientific tools. To do so, they will need to calibrate their stimulation parameters based on the recorded neural response, moving away from heuristic-based stimulation protocols. To achieve single-cell resolution, the interface needs to record the directly elicited spike with low latency after the stimulation (e.g.  $<500 \mu\text{s}$  in an *ex-vivo* monkey retina [1]). Notably, a critical problem towards closed-loop neural modulation is the stimulation artifact, which is the voltage that results from injecting the stimulation current into the large electrode impedance ( $Z_{\text{EL}}$ ). Typically, the resulting stimulation artifact is orders of magnitude larger than the neural signal of interest, obscuring the neural response on the stimulating electrode and its neighboring sites [1]. Also, because of the large time constant associated with  $Z_{\text{EL}}$  and the charge imbalance at the electrode after the stimulation is over, the stimulation artifact can last for several milliseconds [2]. We refer to the artifact during stimulation as the *direct artifact*, and after stimulation as the *residual artifact*. It is important to note that a perfectly charge-balanced stimulation waveform does not necessarily ensure charge balancing at the electrode, due to the electrode-tissue interface (ETI) non-linearity [3]. Also, as we will show below, balancing the charge at the output of the AFE does not ensure that the charge at the electrode is also balanced.

When targeting the directly elicited spike, the direct artifact is not so problematic as recording is not needed during stimulation. Typically, it is sufficient to avoid saturation of the analog front-end (AFE) during stimulation by disconnecting it from the electrode (*blanking*) [4]. However, the residual artifact can still obscure the recording channel during the arrival of the elicited spike. Active discharging can be implemented

to reduce the duration of the residual artifact by shorting the input to a fixed potential (*hard reset*) [5] or shifting the pole of the AFE to a higher frequency (*soft reset*) [6]. However, these methods still blank the AFE for a significant time. Alternatively, a high dynamic-range (DR) AFE can be used to record the superimposed signals [7]–[9] and the artifact can be removed in the digital domain [1], [2]. However, this comes at the cost of increased power and area consumption for the AFE. A very effective and popular method to reduce the required DR is to perform artifact cancellation at the input of the AFE combined with template matching in the digital backend [10]–[12]. This solution significantly improves the power efficiency of the recording channel, but it still requires a low noise cancellation circuit at the input. The resulting overhead can become a limiting factor when trying to massively scale up the number of recording channels.

An interesting alternative is to mitigate the residual artifact by modifying the stimulation waveform to push the artifact to higher frequencies to facilitate filtering in the AFE [13], [14], or to reduce the artifact duration based on equalization techniques [15]. Similar to [15], this paper predistorts the stimulation waveform based on a linear time-invariant (LTI) model of the ETI - Fig. 1(a). However, the proposed approach allows for arbitrary constraints to produce distorted waveforms (*optimum stimulation*) that maintain the effectiveness of stimulation while minimizing the artifact duration (*optimum response*) - Fig. 1(b). It also introduces a low-cost trimming step to account for any errors in the response prediction due to the LTI assumption - Fig. 1(c). We validated the proposed

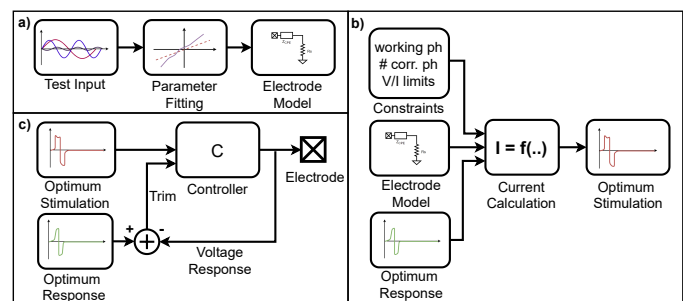


Fig. 1. Proposed fast artifact recovery algorithm (FARA) based on (a) an LTI model of the electrode-tissue interface to (b) design an optimum stimulation waveform for minimum residual artifact duration with (c) a trimming step to account for small errors in the model.

technique in saline solution with a custom PCB based on the Intan RHS2116 chip [16] and a microelectrode array (MEA). In the worst case, the residual artifact duration was reduced to 160  $\mu$ s, which shows an 81% improvement over a triphasic pulse typically used for artifact reduction [17].

Section II describes the ETI model used in this paper. The fast artifact recovery algorithm (FARA) is presented in Section III, while its results are discussed in Section IV.

## II. ELECTRODE-TISSUE INTERFACE MODEL

The electrode-tissue interface is usually modeled by means of an electrode impedance,  $Z_{EL}$ , that describes how electronic current in the stimulator is transduced to ionic current in the tissue. Unfortunately, modeling  $Z_{EL}$  is not a simple task, as the model needs to capture all the electrochemical reactions happening at the interface, some of which are not reversible and voltage dependent. However, for small deviations from the equilibrium potential across  $Z_{EL}$ , negligible irreversible reactions occur, and a linear model can be employed. If linearity holds, electrochemical impedance spectroscopy (EIS) captures the interface behavior accurately and it can be used to predict the artifact shape [18]. In single-cell resolution applications small stimulation currents are typically used, hence, we expect small deviations from the equilibrium potential. For example, [19] shows that the threshold for most neurons in an ex-vivo retina is below 125 pC, which requires only 500 nA if using 250  $\mu$ s pulses.

The impedance model used here is  $Z_{EL} = R_S + Z_{CPE}$ , where  $Z_{CPE} = (As^\alpha)^{-1}$  is referred to as a constant-phase element (CPE), and  $A$  and  $\alpha$  are constants [20]. The constant  $\alpha$  ranges from 0 to 1, where for  $\alpha = 0$ , the CPE is equivalent to a resistor of value  $A^{-1}$ , and for  $\alpha = 1$  the CPE is equivalent to a capacitor of value  $A$ .

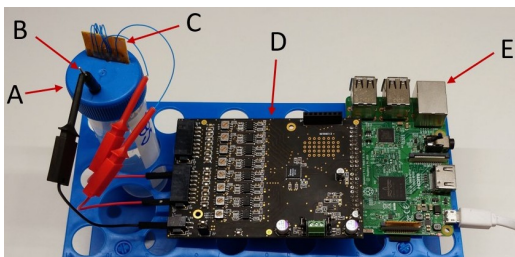
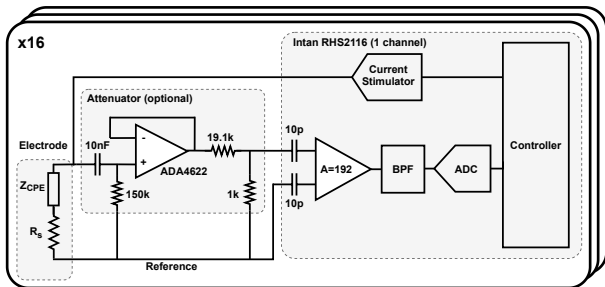


Fig. 2. Experimental setup schematic and photograph. (A) Saline solution, (B) reference electrode, (C) MEA, (D) custom PCB with Intan chip, (E) raspberry Pi microcontroller.

We used the experimental setup in Fig. 2 to test the LTI assumption and perform EIS on the MEA to fit our impedance model. The attenuator in front of the Intan chip is to avoid saturation of the AFE during the direct artifact. This results in an extended input range of  $\pm 100$  mV, while still keeping an input-referred resolution of 4  $\mu$ V which is sufficient for our experiments. The MEA used in this work has gold electrodes with 30  $\mu$ m diameter and 240  $\mu$ m pitch, and it is embedded in a flexible polyurethane substrate.

To assess linearity the artifact is measured for a 250  $\mu$ s pulse with amplitudes ranging from 200 nA to 1200 nA. The normalized input-output relationship shows a linearity deviation of  $<6\%$  across the entire amplitude range. Time-invariance was also verified by recording the artifact when a biphasic 250  $\mu$ s, 1  $\mu$ A pulse is applied [10, 100, 1000] seconds apart, which results in deviations within the noise floor of the system. Hence, we conclude that the system is LTI within the operating range of our application.

EIS on the MEA is performed with the Intan chip in the [0.2-7] kHz range using the recording and stimulation channels - i.e. no dedicated EIS system is used for this measurement. The impedance model parameters  $R_S$ ,  $A$ , and  $\alpha$  are calculated based on the measurement results. Given our impedance model, the time-domain step response is given by:

$$V_{step}(t) = \mathcal{L}^{-1} \left\{ \frac{R_s}{s} \right\} + \mathcal{L}^{-1} \left\{ \frac{1}{As^{\alpha+1}} \right\} \quad (1)$$

$$= \left( R_s + \frac{1}{A} \frac{t^\alpha}{\Gamma(1+\alpha)} \right) u(t) \quad (2)$$

The discrete time step response at sample  $n$ , given a sampling period  $T_s$  and step current magnitude  $\Delta I_0$  is then

$$V_{step}(nT_s) = \Delta I_0 R_s + \frac{\Delta I_0}{A} \frac{T_s^\alpha}{\Gamma(1+\alpha)} n^\alpha \quad (3)$$

where  $\Gamma$  is the gamma function. We can extend this to  $N$  current steps  $\Delta I_i$  to find the voltage response to an arbitrary current waveform. At sample  $k \geq N$  (i.e. only prior current steps contribute), the response is given by

$$V(k) = R_s \sum_{i=1}^N \Delta I_i + \sum_{i=1}^N \{ \Delta I_i K(k-i)^\alpha \}, \quad (4)$$

where  $K = T_s^\alpha / A\Gamma(1+\alpha)$ . FARA uses this estimated response to design an optimal waveform that minimizes the residual artifact. We show that with the only parameters  $R_S$ ,  $K$  and  $\alpha$  we can estimate the voltage response with enough accuracy for our target application - e.g. NMSE = -31.4 dB for a random stimulation waveform (Fig. 3).

## III. FAST ARTIFACT RECOVERY ALGORITHM

FARA uses the model described in Section II to design a stimulation waveform based on the desired optimum response, while meeting specific constraints. Given the desired charge to deliver to the tissue (*working phase*), corrective phases are added to the waveform to minimize the artifact duration. The following constraints are considered here:

- 1) the working phase is not modified by the algorithm,

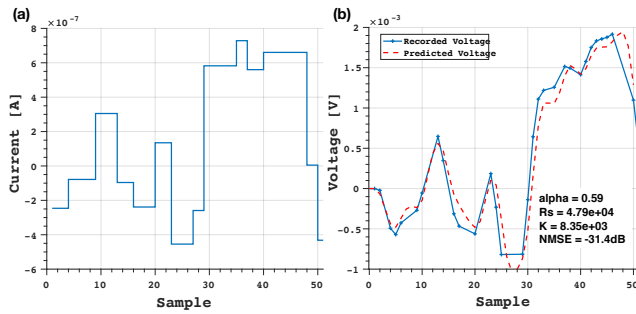


Fig. 3. Model performance. (a) Random current stimulation waveform. (b) Recorded and predicted voltage response.

- 2) maximum limits in the used currents and generated voltages can be applied, and
- 3) corrective phases are always of opposite polarity with respect to the working phase.

In this work, we use an anodic working phase (but the opposite can be implemented), 10 corrective phases before (*pre-correction*) and 5 after (*post-correction*) the working phase, respectively. Each corrective phase is 20  $\mu$ s long.

A possible approach to design the optimum stimulation waveform is to expand Eq. 4 to a matrix form  $V = Z\Delta I$ , and invert matrix  $Z$  to find the required current waveform for the desired voltage response,  $\Delta I = Z^{-1}V$ . The objective is to find the different current steps needed to force the voltage response to zero after the end of the stimulation waveform. However, as the number of degrees of freedom (i.e. corrective phases) increase, the matrix inversion problem becomes too large and results in unstable results. Hence, instead of an explicit solution, an iterative approach is used to find the optimum stimulation waveform.

The implemented iterative approach forces the residual artifact to zero one sample at a time, as new corrective phases are added to the waveform - see Fig. 4 for an illustrative example. This avoids the need for large matrix inversions, and allows for easier implementation of constraints, such as current and voltage limiting. For example, limiting the maximum current to be used will result in a voltage residue. However, subsequent phases can easily account for this, while the matrix inversion approach could not.

The pre-correction and post-correction pulses are used to force the long-term and short-term residual voltage to zero, respectively. To account for their mutual effect, the iterative process is repeated over 5 convergence cycles - see Fig. 4(d).

The proposed algorithm relies on the electrode-tissue interface being an LTI system. Although this assumption is realistic for the small stimulation thresholds in single-cell resolution applications, small non-linearities and inaccuracy in the current output could lead to a residual error in the voltage response. This issue becomes more predominant as the stimulation amplitude increases. Hence, we introduced an optional trimming step that corrects for these errors by adjusting the stimulation waveform based on the recorded voltage response. The trimming algorithm performs a binary

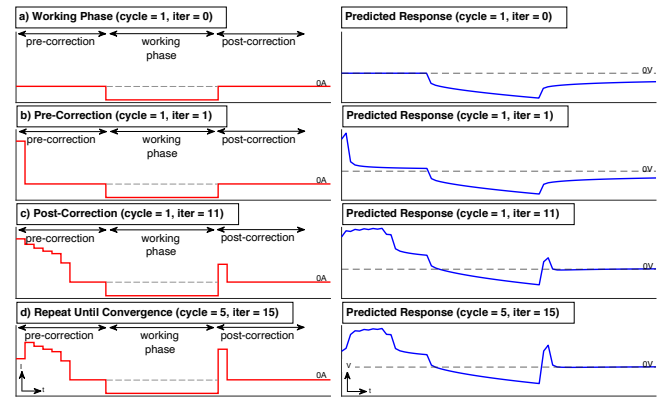


Fig. 4. Iterative approach of the fast artifact recovery algorithm - (left) stimulation current waveform, (right) predicted voltage response, i.e. stimulation artifact.

search to correct for the short-term response first (i.e. post-correction pulses) and the long-term response later (i.e. pre-correction pulses). Experimentally, we found that only 5 trimming iterations are needed for the worst case scenario to reach the optimum response. Given the time-invariance behavior of the ETI, this trimming step is needed only once for each stimulation waveform and its result can be stored for future use.

#### A. Algorithm Cost

The hardware overhead in the recording channels for the proposed algorithm is minimal, as it only requires a blanking technique to avoid saturation during the direct artifact. The trimming step only requires to record the residual artifact, which is already within the input range of the amplifier, so high DR AFEs are not needed. A single high DR AFE can be shared among all channels for the EIS measurement.

The stimulation side requires an arbitrary waveform generator with moderate resolution (e.g. 8 bits are used in the Intan chip for the results reported here), which can also be used for generating the test signals for the EIS measurement. It is important to note that single-cell resolution requires to calibrate the stimulation parameters based on the recorded response, which can become an intractable problem if multiple stimulation channels operate at the same time in the same region. As a result, only a few stimulation channels are used simultaneously, even for massively parallel MEAs [21]. This allows for resource sharing to reduce the system cost of each stimulation channel.

To find the optimum stimulation waveform, FARA predicts the voltage response based on the stimulation current, according to  $V = \Delta I (R_S + Kn^\alpha)$ . We refer to this operation as Model Voltage Calculation (MVC). To reduce the computational cost of each MVC, we limit the range to  $n = 1:100$  (with step 1) and  $\alpha = 0.01:0.99$  (with step 0.01) and store the pre-computed value in a look-up table (LUT). Each MVC requires then one 16-bit addition, two 16-bit multiplications, and one 100x99 LUT inquiry. On average, 3 MVCs are needed per correction phase per convergence cycle. Given 10 pre-

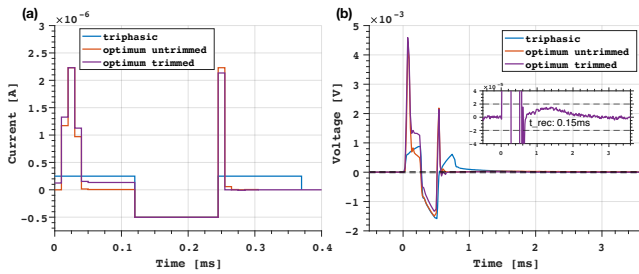


Fig. 5. (a) 250  $\mu$ s, 500 nA pulse using triphasic, untrimmed optimum and trimmed optimum stimulation waveforms. (b) Recorded artifact.

and 5 post-correction phases, and 5 convergence cycles, we need 150 MVCs per waveform optimization. This might not be feasible for the power and area constraints of an implant, especially as the number of channels increase. However, the optimum waveforms can be computed off the implant and transmitted to the stimulation channels as needed. The required data rate for a single waveform, assuming a 100  $\mu$ s working phase, is

$$R = (16ph * 8bit) / (100\mu s + 15ph * 20\mu s) = 320kpbs$$

which is possible based on the data rates demonstrated in recent wireless retinal prostheses [22]–[24]. This is true if we consider that single-cell resolution applications might not stimulate on all channels simultaneously [25].

The trimming step only requires to implement a binary search controlled by the recorded voltage response, and this can be easily implemented on the implant itself.

#### IV. RESULTS

The proposed algorithm was validated in-vitro for different working phase amplitudes (100 nA to 500 nA) and periods (50  $\mu$ s to 250  $\mu$ s). The recovery time is defined as the time from the end of the working phase to the time at which the residual artifact drops below  $\pm 20$   $\mu$ V (approximately twice the input-referred peak-to-peak noise).

To illustrate the behavior of FARA, Fig. 5 shows the stimulation waveform and recorded artifact for a working phase of 250  $\mu$ s, 500 nA when a triphasic, optimum untrimmed and trimmed waveforms are applied. A summary of all tests for the working electrode is provided in Fig. 6(a). The proposed algorithm is compared against mono-, bi-, and tri-phasic waveforms, as well as the active discharge built-in functionality in the Intan chip. The worst-case recovery time is only 160  $\mu$ s, which shows an 81% improvement over a triphasic pulse. It is important to notice that trimming is only necessary for large amplitude phases (i.e.  $>400$  nA), as the proposed model performs well for small deviations from equilibrium at the ETI. Fig. 6(b) shows that the proposed algorithm reduces the artifact duration also at neighboring electrodes ( $d = 240$   $\mu$ m).

We also investigated the effect of the proposed algorithm on the DC accumulated charge at the ETI after 50 consecutive stimulation pulses - see Fig. 6(c). The proposed algorithm results in a larger DC charge accumulated at the ETI when compared to conventional waveforms. This is to be expected

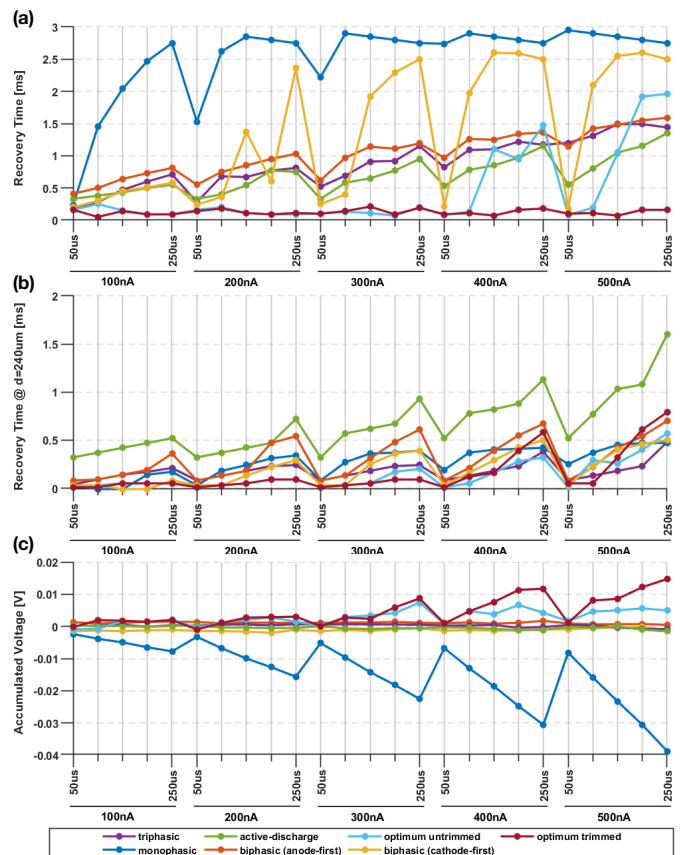


Fig. 6. Recovery time for different stimulation parameters (a) on the working electrode and (b) on the neighboring electrode. (c) DC accumulated voltage at the working electrode after 50 consecutive pulses.

as the algorithm accounts for the AFE transfer function and, hence, minimizes the AC charge at the output of the AFE, and not the DC charge at its input. However, the accumulated charge is always  $<15$  mV, well below the safety thresholds for neural stimulation [26], [27]. Also, single-cell stimulation strategies typically do not employ stimulation pulse trains, as they account for the refractory period of the cell.

#### V. CONCLUSION

This paper presents an optimum stimulation waveform algorithm for artifact fast recovery in single-cell resolution. FARA is designed to work with small stimulation currents, which are always the case in single-cell resolution applications. We show that very fast artifact recovery is possible when properly designing the corrective phases of the stimulation waveform. The proposed algorithm will enable future neural interfaces to record the directly elicited spikes with very low latency. Future work will focus on reducing the algorithm implementation cost to allow for integration directly on the implant.

#### ACKNOWLEDGMENT

We would like to thank V. Giagka, A. Velea, A. Pak, and J. Wilson for providing the MEA for our experiments, and R. van Puffelen for technical support.

## REFERENCES

- [1] G. E. Mena, L. E. Grosberg, S. Madugula, P. Hottowy, A. Litke, J. Cunningham, E. J. Chichilnisky, and L. Paninski, "Electrical stimulus artifact cancellation and neural spike detection on large multi-electrode arrays," *PLoS Comput. Biol.*, vol. 13, no. 11, p. e1005842, Nov. 2017.
- [2] H. Jung, J. Kim, and Y. Nam, "Recovery of early neural spikes from stimulation electrodes using a DC-coupled low gain high resolution data acquisition system," *J. Neurosci. Methods*, vol. 304, pp. 118–125, Jul. 2018.
- [3] M. N. van Dongen and W. A. Serdijn, "Does a coupling capacitor enhance the charge balance during neural stimulation? an empirical study," *Med. Biol. Eng. Comput.*, vol. 54, no. 1, pp. 93–101, Jan. 2016.
- [4] S. Elyahoodayan, W. Jiang, H. Xu, and D. Song, "A Multi-Channel asynchronous neurostimulator with artifact suppression for neural Code-Based stimulations," *Front. Neurosci.*, vol. 13, p. 1011, Sep. 2019.
- [5] P. Hottowy, A. Skoczniak, D. E. Gunning, S. Kachiguine, K. Mathieson, A. Sher, P. Wiacek, A. M. Litke, and W. Dabrowski, "Properties and application of a multichannel integrated circuit for low-artifact, patterned electrical stimulation of neural tissue," *J. Neural Eng.*, vol. 9, no. 6, p. 066005, Dec. 2012.
- [6] V. Viswam, Y. Chen, A. Shadmani, J. Dragas, R. Bounik, R. Milos, J. Muller, and A. Hierlemann, "2048 action potential recording channels with 2.4  $\mu$ Vrms noise and stimulation artifact suppression," 2016.
- [7] C. Kim, S. Joshi, H. Courellis, J. Wang, C. Miller, and G. Cauwenberghs, "Sub- $\mu$  Vrms-Noise sub- $\mu$  W/Channel ADC-Direct neural recording with 200-mV/ms transient recovery through predictive digital autoranging," *IEEE J. Solid-State Circuits*, vol. 53, no. 11, pp. 3101–3110, Nov. 2018.
- [8] H. Jeon, J. Bang, Y. Jung, I. Choi, and M. Je, "A high DR, DC-Coupled, Time-Based Neural-Recording IC with degeneration R-DAC for bidirectional neural interface," *IEEE J. Solid-State Circuits*, vol. 54, no. 10, pp. 2658–2670, Oct. 2019.
- [9] C. Lee, T. Jeon, M. Jang, S. Park, J. Kim, J. Lim, J.-H. Ahn, Y. Huh, and Y. Chae, "A 6.5- $\mu$ W 10-kHz BW 80.4-dB SNDR Gm-C-Based CT  $\Sigma$  modulator with a Feedback-Assisted gm linearization for Artifact-Tolerant neural recording," pp. 2889–2901, 2020.
- [10] A. E. Mendrela, J. Cho, J. A. Fredenburg, V. Nagaraj, T. I. Netoff, M. P. Flynn, and E. Yoon, "A bidirectional neural interface circuit with active stimulation artifact cancellation and Cross-Channel Common-Mode noise suppression," *IEEE J. Solid-State Circuits*, vol. 51, no. 4, pp. 955–965, Apr. 2016.
- [11] J. Uehlin, W. A. Smith, V. Rajesh Pamula, S. Perlmutter, V. Sathe, and J. C. Rudell, "A bidirectional brain computer interface with 64-channel recording, resonant stimulation and artifact suppression in standard 65nm CMOS," in *ESSCIRC 2019 - IEEE 45th European Solid State Circuits Conference (ESSCIRC)*, Sep. 2019, pp. 77–80.
- [12] S. Culaclic, B. Kim, Y.-K. Lo, L. Li, and W. Liu, "Online artifact cancellation in Same-Electrode neural stimulation and recording using a combined hardware and software architecture," *IEEE Trans. Biomed. Circuits Syst.*, vol. 12, no. 3, pp. 601–613, Jun. 2018.
- [13] L. F. Heffer and J. B. Fallon, "A novel stimulus artifact removal technique for high-rate electrical stimulation," *J. Neurosci. Methods*, vol. 170, no. 2, pp. 277–284, May 2008.
- [14] B. Dura, M. Q. Chen, O. T. Inan, G. T. A. Kovacs, and L. Giovangrandi, "High-frequency electrical stimulation of cardiac cells and application to artifact reduction," *IEEE Trans. Biomed. Eng.*, vol. 59, no. 5, pp. 1381–1390, May 2012.
- [15] P. Chu, R. Muller, A. Koralek, J. M. Carmena, J. M. Rabaey, and S. Gambini, "Equalization for intracortical microstimulation artifact reduction," *Conf. Proc. IEEE Eng. Med. Biol. Soc.*, vol. 2013, pp. 245–248, 2013.
- [16] Intan Technologies. [https://intantech.com/products\\_RHS2000.html](https://intantech.com/products_RHS2000.html).
- [17] A. Bahmer, O. Peter, and U. Baumann, "Recording and analysis of electrically evoked compound action potentials (ECAPs) with MED-EL cochlear implants and different artifact reduction strategies in matlab," *J. Neurosci. Methods*, vol. 191, no. 1, pp. 66–74, Aug. 2010.
- [18] Z. C. Chen, B.-Y. Wang, and D. Palanker, "Harmonic-balance circuit analysis for electro-neural interfaces," *Journal of neural engineering*, vol. 17, no. 3, p. 035001, Jun. 2020.
- [19] L. H. Jepson, P. Hottowy, K. Mathieson, D. E. Gunning, W. Dabrowski, A. M. Litke, and E. J. Chichilnisky, "Focal electrical stimulation of major ganglion cell types in the primate retina for the design of visual prostheses," *Journal of Neuroscience*, vol. 33, no. 17, pp. 7194–7205, Apr. 2013.
- [20] J. Lario-García and R. Pallàs-Areny, "Constant-phase element identification in conductivity sensors using a single square wave," *Sens. Actuators A Phys.*, vol. 132, no. 1, pp. 122–128, Nov. 2006.
- [21] D. G. Muratore and E. J. Chichilnisky, "Artificial retina: A future Cellular-Resolution Brain-Machine interface," in *NANO-CHIPS 2030: On-Chip AI for an Efficient Data-Driven World*, B. Murmann and B. Hoefflinger, Eds. Cham: Springer International Publishing, 2020, pp. 443–465.
- [22] K. Chen, Y.-K. Lo, and W. Liu, "A 37.6 mm 2 1024-channel high-compliance-voltage SoC for epiretinal prostheses," in *2013 IEEE International Solid-State Circuits Conference Digest of Technical Papers*, 2013, pp. 294–295.
- [23] M. Monge, M. Raj, M. Honarvar-Nazari, H.-C. Chang, Y. Zhao, J. Weiland, M. Humayun, Y.-C. Tai, and A. Emami-Neyestanak, "A fully intraocular 0.0169 mm<sup>2</sup>/pixel 512-channel self-calibrating epiretinal prosthesis in 65nm CMOS," in *2013 IEEE International Solid-State Circuits Conference Digest of Technical Papers*, 2013, pp. 296–297.
- [24] W. Lemaire, M. Benhouria, K. Koua, M. Besrou, L.-P. Gauthier, G. Martin-Hardy, T. Rossignol, S. Roy, and R. Fontaine, "Retinal stimulator ASIC architecture based on a joint power and data optical link," *IEEE J. Solid-State Circuits*, vol. 56, no. 7, pp. 2158–2170, Jul. 2021.
- [25] N. P. Shah, S. Madugula, L. Grosberg, G. Mena, P. Tandon, P. Hottowy, A. Sher, A. Litke, S. Mitra, and E. J. Chichilnisky, "Optimization of electrical stimulation for a High-Fidelity artificial retina," 2019.
- [26] D. R. Merrill, M. Bikson, and J. G. R. Jefferys, "Electrical stimulation of excitable tissue: design of efficacious and safe protocols," *Journal of Neuroscience Methods*, vol. 141, no. 2, pp. 171–198, Feb. 2005.
- [27] S. F. Cogan, "Neural stimulation and recording electrodes," *Annual Review of Biomedical Engineering*, vol. 10, pp. 275–309, 2008.